How to cite: Angew. Chem. Int. Ed. 2024, e202417027
doi.org/10.1002/anie.202417027

Cancer Therapy

Bifunctional Metal–Organic Framework Synergistically Enhances Radiotherapy and Activates STING for Potent Cancer Radio-Immunotherapy

Chaoyu Wang[+], Jinhong Li[+], Xiaomin Jiang[+], Xin Ma, Wenyao Zhen, Langston Tillman, Ralph R. Weichselbaum, and Wenbin Lin**

Abstract: The activation of the stimulator of interferon genes (STING) protein by cyclic dinucleotide metabolites plays a critical role in antitumor immunity. However, synthetic STING agonists like 4-(5,6-dimethoxybenzo[b]thiophen-2-yl)-4-oxobutanoic acid (MSA-2) exhibit suboptimal pharmacokinetics and fail to sustain STING activation in tumors for effective antitumor responses. Here, we report the design of MOF/MSA-2, a bifunctional MSA-2 conjugated nanoscale metal–organic framework (MOF) based on Hf_6 secondary building units (SBUs) and hexakis(4′-carboxy[1,1′-biphenyl]-4-yl)benzene bridging ligands, for potent cancer radioimmunotherapy. By leveraging the high-Z properties of the Hf_6 SBUs, the MOF enhances the therapeutic effect of X-ray radiation and elicits potent immune stimulation in the tumor microenvironment. MOF/MSA-2 further enhances radiotherapeutic effects of X-rays by enabling sustained STING activation and promoting the infiltration and activation of immune cells in the tumors. MOF/MSA-2 plus low-dose X-ray irradiation elicits strong STING activation and potent tumor regression, and when combined with an immune checkpoint inhibitor, effectively suppresses both primary and distant tumors through systemic immune activation.

[*] Dr. C. Wang,[+] J. Li,[+] Dr. X. Jiang,[+] Dr. X. Ma, Dr. W. Zhen, L. Tillman, Prof. Dr. W. Lin
Department of Chemistry
The University of Chicago
929 E 57th St, Chicago, IL 60637, USA
E-mail: wenbinlin@uchicago.edu

Dr. C. Wang,[+] Dr. X. Jiang,[+] Dr. W. Zhen, Prof. Dr. R. R. Weichselbaum, Prof. Dr. W. Lin
Department of Radiation and Cellular Oncology and Ludwig Center for Metastasis Research
The University of Chicago
5758 S Maryland Ave, Chicago, IL 60637, USA
E-mail: rweichselbaum@uchicagomedicine.org

[+] These authors contributed equally to this work.

Introduction

Radiotherapy (RT) is a cornerstone in cancer treatment, with approximately half of cancer patients receiving RT during their courses of disease management. RT works by using ionizing radiation to damage the DNA of cancer cells, effectively killing them or inhibiting their ability to reproduce.[1] However, RT has significant clinical limitations, including debilitating side effects from high doses of radiation, radioresistance, and the inability to effectively target metastatic lesions that are beyond the irradiated tumors.[2] High radiation doses are needed to eradicate tumors due to the low radiosensitivity of many tumors, which causes significant damage to normal tissues and serious side effects in cancer patients. Radioresistance allows tumor cells to withstand radiation, reducing treatment efficacy and leading to cancer recurrence. The inability of RT to control metastatic lesions that are beyond the irradiated field limits its effectiveness against advanced cancers. These challenges highlight the critical need for innovative strategies to significantly enhance RT efficacy.

Chemotherapy administered in combination with RT has been clinically used to enhance therapeutic effects against many cancers including head and neck cancer, rectal cancer, and cervical cancer, but this combination often causes serious side effects to cancer patients.[3] Radiosensitizers have also been examined to enhance the effects of RT,[4] but none has been approved for clinical use by the US Food and Drug Administration. RT has been shown to foster an immunosuppressive tumor microenvironment (TME) by promoting the accumulation of myeloid-derived suppressor cells (MDSCs), enhancing the activity of the nuclear factor kappa-light-chain-enhancer of activated B cells (NF-κB), and causing the exhaustion of lymphoid cells.[5] Existing radiosensitizers enhance DNA double-strand breaks (DSBs) but do not sufficiently overcome the immunosuppressive TME, thus limiting their ability to enhance the efficacy of RT without sufficiently engaging the patient's immune system to target and destroy tumor cells.[6] To address the limitations of existing radiosensitizers, we have examined nanoscale metal–organic frameworks (MOFs) as a new class of radioenhancers via increasing radiation absorption and promoting reactive oxygen species (ROS) generation[7] as well as by creating an immunostimulatory TME. A MOF-

based radioenhancer has shown preliminary anticancer efficacy when combined with low-dose radiation in a phase 1 clinical trial.[8] We hypothesized that the porosity and cargo loading ability of MOFs can be leveraged to deliver small molecule immunotherapeutics to further enhance the therapeutic efficacy of ionizing radiation via synergistic radioenhancement and immune activation.

The STING agonist 4-(5,6-dimethoxybenzo-[b]thiophen-2-yl)-4-oxobutanoic acid (MSA-2) is a novel immunotherapeutic drug candidate that stimulates a robust anti-tumor immune response by activating the STING pathway to promote the production of interferons and other cytokines.[9] MSA-2 has shown potential therapeutic effects on multiple types of tumors.[9b] However, MSA-2 has suboptimal pharmacokinetic properties, such as low bioavailability, rapid metabolism in vivo, and uneven distribution, which limit its effectiveness and application in cancer treatment.[10] As a result, suitable nanocarriers are needed to increase intratumoral MSA-2 concentration, protect it from premature metabolism, and sustain its release in the tumors to realize its therapeutic potential.

Here, we report the design of MOF/MSA-2, a bifunctional MSA-2 conjugated nanoscale MOF based on Hf_6 secondary building units (SBUs) and hexakis(4′-carboxy[1,1′-biphenyl]-4-yl)benzene (HCBB) bridging ligands, for potent cancer radio-immunotherapy. The MOF leverages the high-Z properties of the Hf_6 SBUs to enhance the therapeutic effect of X-ray radiation,[11] and provides anchoring sites for MSA-2 loading. MOF/MSA-2 sustains the release of MSA-2 in tumors to elicit strong and durable STING activation. The synergistic action of MOF-mediated RT and STING activation by MSA-2 effectively regressed local tumors and activated the tumor immune environment in two murine colorectal cancer (CRC) models. Further combination with an anti-PD–L1 antibody (αPD–L1) showed improved distant tumor control as manifested by an abscopal effect on a bilateral CRC model[11a,12] extending the local treatment of MOF/MSA-2 to systemic antitumor immune responses.

Results and Discussion

Synthesis and Characterization of MOF/MSA-2

The Hf-HCBB nanoscale MOF (abbreviated as the MOF in this article) comprising Hf_6 SBUs and HCBB bridging ligands (Figure S3) was synthesized via a solvothermal reaction of $HfCl_4$ and H_6HCBB in a mixture of N,N-dimethylformamide (DMF), acetic acid, and water at 80 °C (Figure 1a). Powder X-ray diffraction (PXRD) showed that the nanoscale MOF is isostructural to the previously reported pbz-MOF-1 based on Zr_6 SBUs and

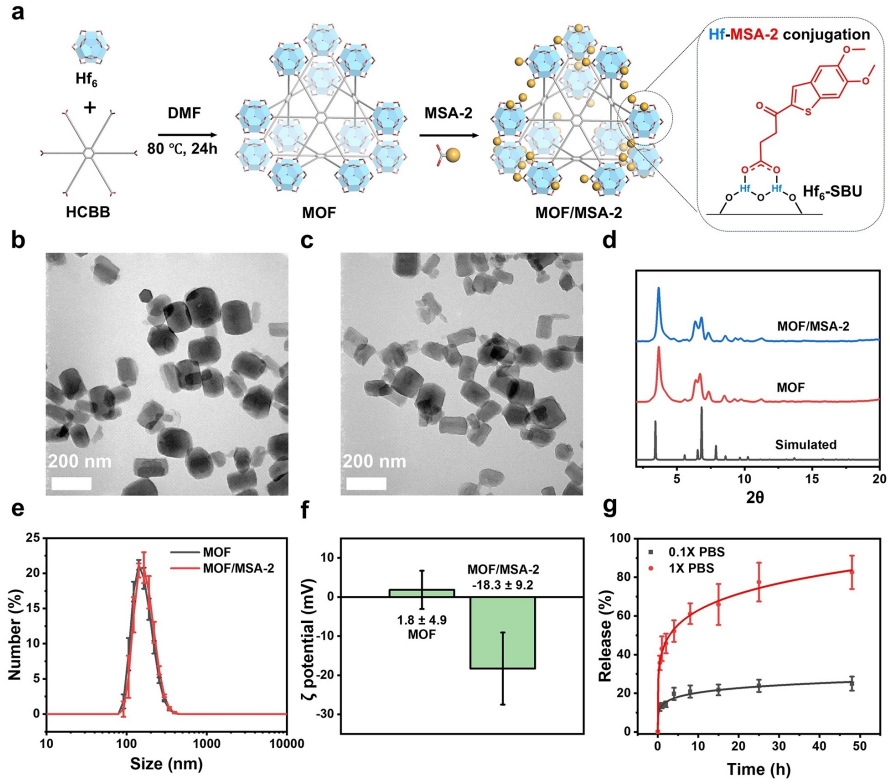

Figure 1. (a) Schematic showing the synthesis of MOF and MOF/MSA-2. (b,c) TEM images of Hf-MOF (b) and MOF/MSA-2 (c). Scale bar = 200 nm. (d) PXRD patterns of MOF and MOF/MSA-2, along with the simulated pattern for the MOF. (e) Number-averaged sizes of MOF and MOF/MSA-2 in water. (f) Zeta potentials of MOF and MOF/MSA-2 in water. (g) Release percentages of MSA-2 from MOF/MSA-2 in 0.1×PBS or 1×PBS, respectively ($n = 3$).

HCBB bridging ligands (Figure 1b).[13] Transmission electron microscopy (TEM) imaging of the MOF demonstrated a cubic morphology (Figure 1c), while dynamic light scattering (DLS) measurements provided a number-averaged particle size of 190.4 ± 3.3 nm for the MOF (Figure 1e). The surface charge of the MOF was determined to be nearly neutral, with a ζ-potential of 1.8 ± 4.9 mV in water (Figure 1f). ^{1}H NMR and inductively coupled plasma-mass spectroscopic (ICP-MS) analyses of the digested MOF afforded an empirical formula of $[Hf_6(\mu_3\text{-}O)_4(\mu_3\text{-}OH)_4(OH)_6(H_2O)_6(HCBB)](CH_3CO_2H)_{1.4}$ which is consistent with the structure of pbz-MOF-1 (Figure S1a, S2b, S4, S5).

As we have previously shown that the $^-OH/H_2O$ groups on the SBUs of Hf MOFs can be replaced by carboxy-containing functional molecules,[14] we hypothesized that the $^-OH/H_2O$ groups in the MOF could be replaced by MSA-2. Due to the presence of six $^-OH/H_2O$ groups on each Hf_6 SBU, the MOF is expected to have a high loading of MSA-2.[15] MOF/MSA-2 was synthesized by heating a mixture of MOF and MSA-2 in ethanol at 50 °C for 24 h (Figure 1a). TEM and DLS analyses confirmed that MOF/MSA-2 retained the cubic morphology and size (195.36 ± 2.2 nm) of the MOF (Figure 1c, 1f). The PXRD pattern of MOF/MSA-2 was nearly identical to that of the MOF (Figure 1d), indicating the maintenance of the MOF structure after MSA-2 loading. MOF/MSA-2 exhibited a markedly more negative ζ-potential of −18.3 ± 9.2 mV (Figure 1e). UV–vis, ^{1}H NMR, and ICP-MS analyses of the digested MOF/MSA-2 revealed a molecular formula of $[Hf_6(\mu_3\text{-}O)_4(\mu_3\text{-}OH)_4(OH)_{2.4}(H_2O)_{2.4}\text{-}(MSA)_{3.6}(HCBB)](CH_3CO_2H)_{0.4}$ (Figure S5). These results indicate the loading of 29.2 wt % of MSA-2 in MOF/MSA-2.

We next determined the replacement of carboxylate capping groups of MSA-2 on MOF/MSA-2 by phosphate ions under physiological conditions. The release profiles of MSA-2 from MOF/MSA-2 were determined by liquid chromatography-mass spectrometry (LC–MS) in 0.1× and 1× phosphate-buffered saline (PBS) solutions to mimic extracellular conditions and intracellular phosphate concentration conditions, respectively (Figures 1g, S1b). MOF/MSA-2 released 25.0 % and 82.6 % MSA-2 in 0.1× and 1× PBS, respectively, in 48 hours. Thus, MOF/MSA-2 showed a 3.3-times higher MSA-2 release in 1× PBS over 0.1× PBS, indicating the ability of MOF/MSA-2 to release MSA-2 intracellularly in response to the elevated intracellular phosphate concentrations.

MOF Enhances Radiotherapy and Induces Immunogenic Cell Death

We first used the DCFH-DA probe to detect total ROS generation in murine colon cancer CT26 cells.[16] To evaluate ROS generation by MOF plus 2 Gy irradiation [denoted MOF(+)], we incubated CT26 cells with the MOF for 24 h and then replaced the medium with fresh medium containing the DCFH-DA probe, which became fluorescent after oxidation by ROS (Figure 2a, Figure S2a). Laser scanning confocal microscopy (LSCM) showed that MOF(+) induced more intracellular ROS than PBS(+), which was evenly distributed in CT26 cells. In contrast, PBS and MOF groups did not increase ROS. This result shows that MOF(+) efficiently generates ROS in CT26 cells due to the radioenhancement effect of the MOF. The radioenhancement effect of the MOF was also supported by the increased DNA DSBs in CT26 cells. After incubation with the MOF for 24 h followed by 1 Gy or 2 Gy X-ray irradiation, the MOF(+) group showed significant upregulation of phosphorylated histone H2 A.X (γ-H2AX) over PBS(+) groups as quantified by western blot (by 1.7- and 1.9-folds, respectively, Figure 2c) and visualized by LSCM (Figure 2b). The corresponding uncropped images in Figure 2c are included in Figure S18. This result shows that MOF(+) treatments induce more DNA DSBs than PBS(+) treatments due to the potent radioenhancement effect of the MOF.

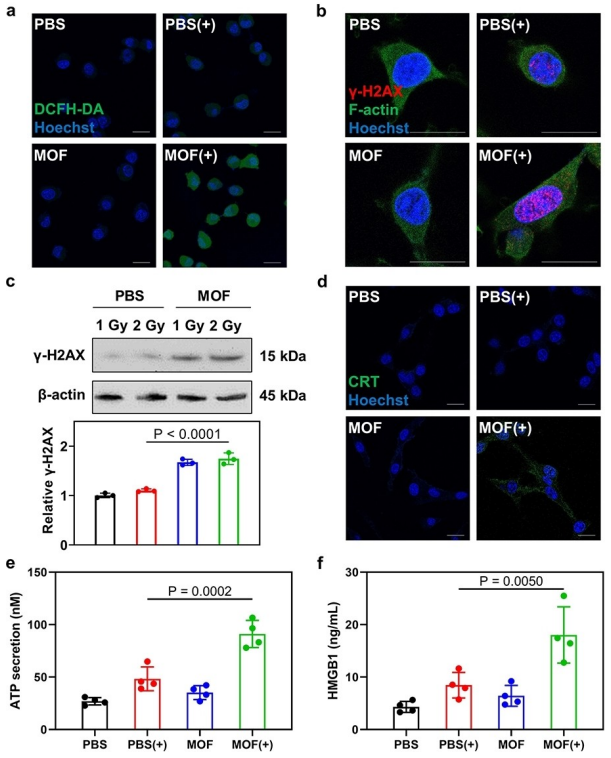

Figure 2. (a) Confocal images showing ROS generation in CT26 cells induced by MOF with or without 2 Gy of X-rays. Scale bars, 10 μm. (b,c) Nuclear DNA DSBs visualized by confocal microscopy (b) and quantified by western blot (c) 24 h after irradiation of CT26 cells with 2 Gy X-rays. The upregulation of γ-H2AX of MOF(+)-treated CT26 cells indicated more DNA DSBs caused by ionizing radiation and hence strong radiosensitization in vitro. Scale bars, 10 μm. F-actin (green) was stained to show cellular morphology. (d) Confocal images showing the upregulation of CRT in CT26 cells induced by MOF with or without 2 Gy of X-rays. Scale bars, 10 μm. (e) ATP secretion from MC38 cells after different treatments. ANOVA with Tukey test, $n = 4$. (f) HMGB1 release from MC38 cells after different treatments. ANOVA with Tukey test, $n = 4$.

In addition to enhancing radiotherapeutic effects of RT, the MOF also enhances ROS-mediated immunogenic cell death (ICD) of cancer cells to expose danger-associated molecular patterns (DAMPs) and tumor-associated antigens (TAAs).[11b,17] After incubation of CT26 cells with the MOF for 24 h followed by 2 Gy irradiation, the MOF(+) group showed significantly higher translocation of calreticulin (CRT) to cell membranes than the PBS(+) group.[18] Incubation of CT26 cells with the MOF or PBS alone did not show any CRT signal (Figure 2d). Additionally, MOF(+) induced adenosine triphosphate (ATP) secretion (Figure 2e) and high mobility group box 1 (HMGB1) release (Figure 2f) in CT26 cells, with 3.4- and 4.2-fold higher ATP and HMGB1 levels, respectively, than PBS, and with 1.9- and 2.1-fold higher ATP and HMGB1 levels, respectively, than PBS(+). These results indicate efficient ICD induction of CT26 tumor cells by the MOF(+) treatment.

MOF/MSA-2 Induces Robust and Sustained STING Activation

We next used THP-1 cells with incorporated IFN-stimulated genes as reporter cells to determine if MOF/MSA-2 could induce STING activation.[17] While free MSA-2 showed a half-maximal effective concentration (EC_{50}) of 69.1 μM for interferon regulatory factor (IRF) response in THP-1 cells, MOF/MSA-2 exhibited a 6.3-fold lower EC_{50} of 10.9 μM. This result demonstrates MOF/MSA-2 as a more potent STING agonist than free MSA-2 (Figure 3a).

Based on the EC_{50} value of MOF/MSA-2, we used an equivalent MSA-2 concentration of 10 μM in subsequent in vitro experiments. We examined the phosphorylation of STING (p-STING) and IRF-3 (p-IRF-3) in Raw264.7 cells as a measure of downstream signals of STING activation.[2a,16a,17] Raw264.7 cells were incubated with PBS, free MSA-2, or MOF/MSA-2 for 24 h and irradiated with 0 or 2 Gy X-rays, and then cultured for another 24 hours. MOF/MSA-2(+) treatment upregulated 3.4-, 3.6-, 2.7-, and 2.4-fold higher p-STING and 2.3-, 2.1-, 1.4-, and 1.9-fold higher p-IRF-3 than PBS, MSA-2, MSA-2(+), and MOF/MSA-2 treatments, respectively (Figure 3b). The corresponding uncropped images in Figure 3b are included in Figure S19. Next, LSCM was used to assess time-dependent STING activation in Raw264.7 cells. While free MSA-2 induced phosphorylation of STING and phosphorylation IRF-3 in 2 h, the p-STING and p-IRF-3 signals quickly disappeared in 12 h (Figure 3c and Figure 3d), likely due to rapid metabolic degradation of free MSA-2. In contrast, MOF/MSA-2 elicited a sustained and strong STING phosphorylation and IRF-3 phosphorylation with p-STING and p-IRF-3 signals increasing steadily throughout 24 h and higher p-STING signals than MSA-2 at 24 h post-treatment (Figure 3c and Figure 3d).

We further showed that MOF/MSA-2(+) induced the secretion of type I interferons (IFNs) and other inflammatory cytokines in immune cells.[11a,19] After MOF/MSA-2(+) treatment, Raw264.7 cells showed a rapid release of

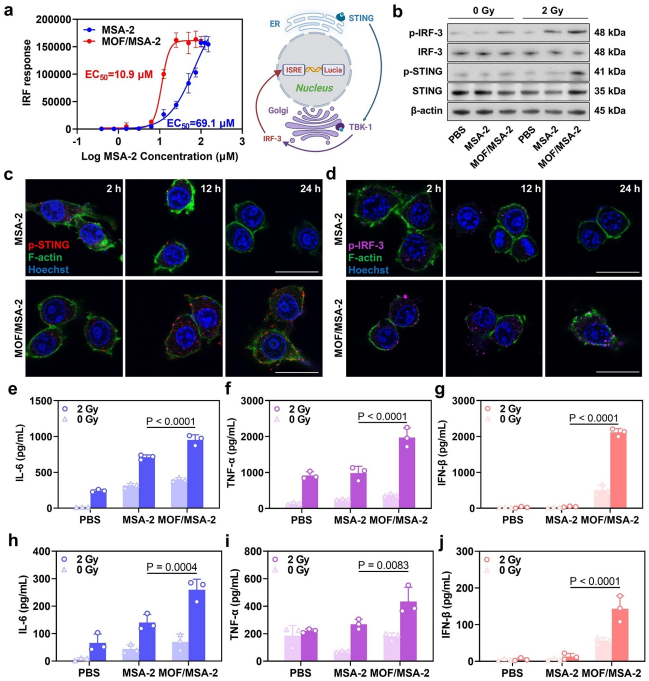

Figure 3. (a) IRF responses on THP-1 reporter cells stimulated by MSA-2 and MOF/MSA-2. The Scheme shows the STING-TBK-IRF-ISRE-Lucia pathway for generating luminescence signals in THP-1 reporter cells. (b) Western blot results showing enhanced STING activation with stronger p-STING and p-IRF-3 signals in Raw264.7 cells by MOF/MSA-2 plus 2 Gy X-rays. (c) Confocal images showing higher expression of p-STING (red) in macrophages (green, labeled by phalloidin) by MOF/MSA-2 over MSA-2 at different time points. (d) Confocal microscopy showing higher expression of p-IRF-3 (purple) in macrophages (green, labeled by phalloidin) by MOF/MSA-2 over MSA-2 at different time points. All scale bars are 20 μm. (e–g) Secretion levels of IL-6 (e), TNF-α (f), and IFN-β (g) by MOF/MSA-2(+) treated Raw264.7 cells. ANOVA with Tukey test, $n=3$. (h–j) Secretion levels of IL-6 (h), TNF-α (i), and IFN-β (j) by MOF/MSA-2(+) treated BMDCs. ANOVA with Tukey test, $n=3$. TBK, TANK-binding kinase. ISRE, interferon-stimulated response element. Lucia, luciferase reporter gene system. The scheme was created with BioRender.com.

interleukin 6 (IL-6) (952.7 ± 58.7 pg/mL, Figure 3e) while BMDCs also continuously secreted IL-6 (259.9 ± 31.2 pg/mL, Figure 3h).[20] MSA-2 had negligible effects, likely due to its low cellular uptake and fast metabolic degradation. Upon MOF/MSA-2(+) treatment, Raw264.7 and BMDCs also showed enhanced secretion of tumor necrosis factor α (TNF-α) (1973.63 ± 217.8 and 434 ± 84.4 pg/mL, respectively, Figure 3f and Figure 3i) and IFN-β over other treatments (2112.1 ± 86.3 and 143.4 ± 28.7 pg/mL, respectively, Figure 3g and Figure 3j).[21] Taken together, MOF/MSA-2(+) elicits stronger and sustained activation of STING and secretion of inflammatory cytokines over MSA-2(+).[22]

MOF/MSA-2 Elicits Potent Therapeutic Effects and Activates the Tumor Microenvironment

The promising in vitro activity of MOF/MSA-2(+) motivated us to explore their therapeutic effects in vivo. Subcutaneous CT26 tumors were established in BALB/c mice by injecting CT26 cells into the right flanks of the mice. Nine days post CT26 cell inoculation, the mice were intratumorally injected with PBS, MSA-2, MOF, or MOF/MSA-2 at an equivalent MOF dose of 1.2 mmol (based on HCBB) or/and MSA-2 dose of 0.5 mg and irradiated with 2 Gy X-rays to the tumor regions on 3 consecutive days (Figure 4a). At this low dose of X-rays, PBS(+) failed to control tumor growth but MSA-2, MOF(+), and MSA-

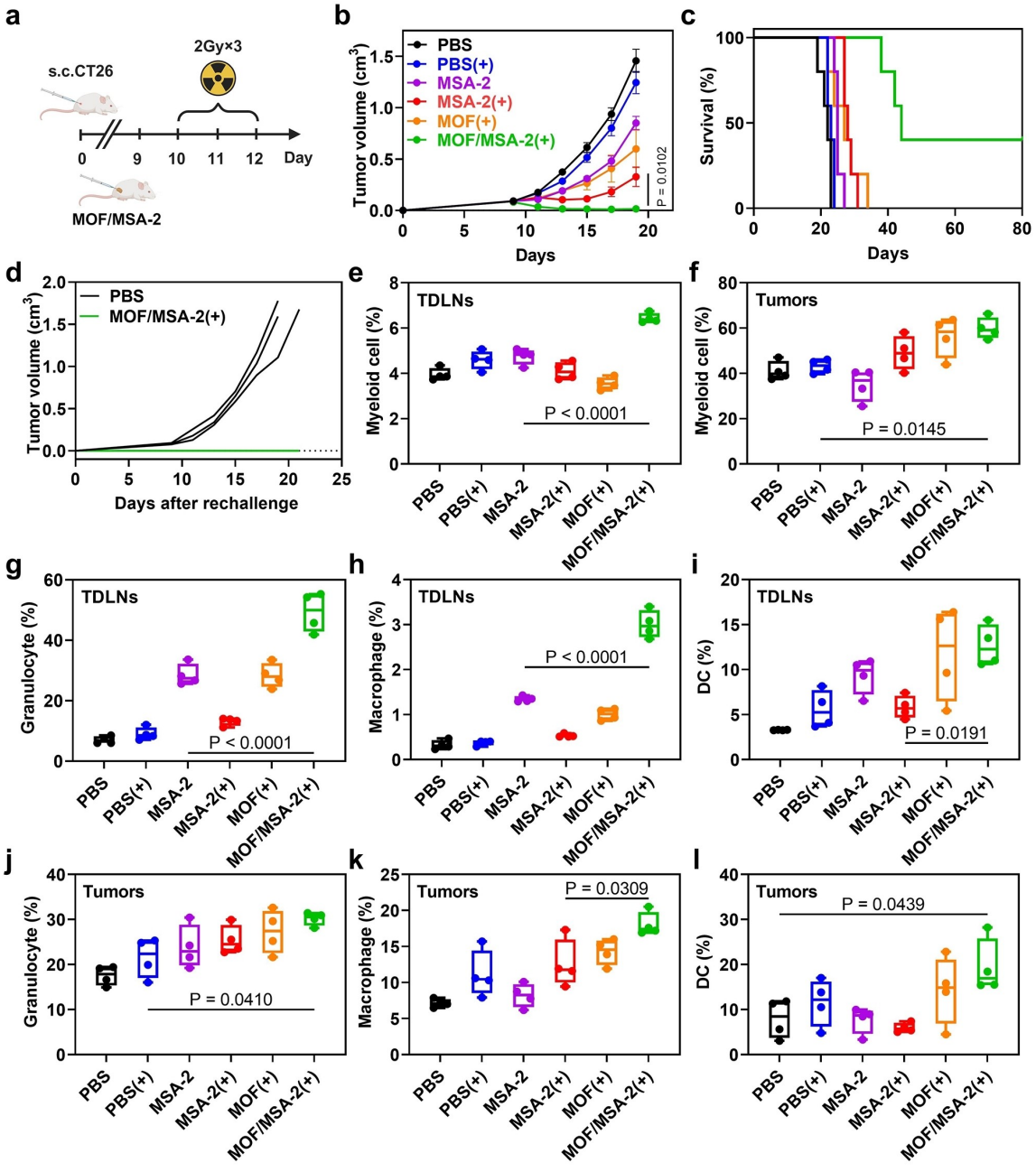

Figure 4. (a) Scheme showing tumor inoculation and treatment schedules. Treatments were intratumorally injected and 2 Gy/fraction was given on 3 consecutive days starting on day 9. (b) Growth curves of subcutaneous CT26 tumors in BALB/c. ANOVA with Tukey test, $n=5$. (c) Mouse survival curves after different treatments. (d) Tumor growth curves after rechallenge with CT26 cells. $n=3$ mice for naïve mouse control and $n=2$ mice for MOF/MSA-2(+) treated mice. (e–l) Immune cell infiltration in the TDLNs and tumors on day 13 (1 day after the last dose of X-ray) quantified by fluorescence-activated cell sorting. The subpopulations were defined as: (e-f) Myeloid cells as $CD45^+CD11b^+$; (g,j) Granulocytes/MDSC as $CD45^+CD11b^+GR\text{-}1^+F4/80^{med}$; (h,k) Macrophages as $CD45^+CD11b^+GR\text{-}1^-F4/80^{high}$; (i,l) Dendritic cells as $CD45^+CD11b^+CD11c^+MHCII^+$. ANOVA with Tukey test, $n=4$. The scheme was created with BioRender.com.

2(+) moderately inhibited tumor growth with tumor growth inhibition (TGI) indices of 41.6 %, 58.9 %, and 77.6 %, respectively. Strikingly, MOF/MSA-2(+) potently regressed tumors with a TGI of 98.9 % and 40 % of tumor-free mice (Figure 4b, and Figure S8). These results show that the MOF act as a strong radioenhancer and MOF-mediated RT further enhances MSA-2 to elicit a strong therapeutic effect.

The mice receiving MOF/MSA-2(+) treatment had longer median survival than those in other treatment groups and doubled median survival over those in PBS control group (Figure 4c). To test if the cured mice have acquired long-term protection against tumor cells,[23] we rechallenged the two tumor-free mice in the MOF/MSA-2(+) group with CT26 cells on day 60 post the initial tumor inoculation. The two tumor-free mice in the MOF/MSA-2(+) group did not develop tumors when the naïve mice reached their tumor burden endpoint (Figure 4d). This result shows that MOF/MSA-2(+) treatment elicits immune memory effect against tumor rechallenge.

To investigate the innate immune response, we profiled leukocytes in the tumors and tumor-draining lymph nodes (TDLNs) two days after the last X-ray irradiation by flow cytometry. MOF/MSA-2(+) treatment decreased total $CD45^+$ leukocytes in the tumors but increased total $CD45^+$ leukocytes in the TDLNs (Figure S9). MOF/MSA-2(+) treatment caused the accumulation of $Gr\text{-}1^+F4/80^{med}$ myeloid cells including granulocytes and myeloid-derived suppressor cells (MDSCs) and the infiltration of $F4/80^{high}$ macrophages and $CD11c^+MHCII^+$DCs in the tumors (Figure 4e, 4f, 4g, 4j). In the TDLNs, MOF/MSA-2(+) treatment induced an obvious increase of macrophages and a higher percentage of DCs (Figure 4h, 4i, 4k, 4l). These observations demonstrate that the synergistic actions of MOF-mediated RT and STING activation by MSA-2 in MOF/MSA-2(+) treatment enhance inflammatory responses in the TME and TDLNs. MOF/MSA-2(+) treatment did not increase $CD8^+$ T cell populations in the tumors and the TDLNs (Figure S10), indicating that the early immune responses are mediated by innate immunity.

MOF/MSA-2 Plus RT in Combination with αPD-L1 Eliminates Bilateral Tumors

We next evaluated the therapeutic efficacy of MOF/MSA-2(+) on bilateral MC38 tumors in C57BL/6 mice, which have been widely used to mimic the clinical treatment of advanced tumors with metastatic lesions. MOF/MSA-2 or PBS was injected into the primary tumors of a bilateral MC38 tumor model at an equivalent MSA-2 dose of 0.5 mg and MOF dose of 1.2 mmol on day 8. The primary tumors were irradiated with 2 Gy/fraction of X-rays on four consecutive days starting on day 9. The mice in the indicated groups were injected intraperitoneally with αPD–L1 at a dose of 75 mg per mouse on days 7 and 11 (Figure 5a).

MOF/MSA-2(+) inhibited the tumor growth but did not regress the primary tumors, and only had a modest inhibitory effect on the distance tumors, with TGI indices of 84.4 % and 52.3 %, respectively (Figure 5b, 5c). Similarly, αPD–L1(+) exhibited a modest inhibitory effect on both primary and distant tumors, with TGI indices of 74.8 % and 61.3 %, respectively. Remarkably, MOF/MSA-2(+)+αPD–L1 treatment regressed both primary and distant tumors with TGI indices of 97.8 %, and 94.3 %, respectively (Figure 5b, 5c). 60 % of the mice were free of tumors on day 21. Consistent with the strong antitumor effects of MOF/MSA-2(+)+αPD–L1 treatment, the mice in this group more than doubled the survival over other groups (Figure S11a). To test if the mice have acquired long-term protection, the three tumor-free mice from the MOF/MSA-2(+)+αPD–L1 group were rechallenged with MC38 cells on day 60. They did not develop MC38 tumors over 21 days while the concurrently treated naive mice all developed tumors and reached tumor burden endpoint over 21 days (Figure S11b).

To investigate the mechanism of systemic immune responses, we profiled immune cells at a later timepoint (Day 17).[24] MOF/MSA-2(+)+αPD–L1 treatment significantly increased the percentages of $CD8^+$, $CD4^+$, and effector T cells, NK cells, and NKT cells in the primary tumors (Figure 5d-i), but only slightly increased these cell populations in the distant tumors (Figure S12). MOF/MSA-2(+)+αPD–L1 treatment also enhanced the infiltration of B cells in both primary and distant tumors (Figure S13). This result shows that combination with αPD–L1 reverses immunosuppression to enhance antitumor immunity.[25]

Whole tumor immunohistochemistry (IHC) staining results showed that MOF/MSA-2(+)+αPD–L1 treatment increased the signals of ionized-calcium binding adaptor molecule 1 (IBA-1) and CD3, the biomarkers for innate and adaptive immune cells, respectively, in the primary tumors (Figure 6a). This result supports enhanced immune infiltration into the TME by the MOF/MSA-2(+)+αPD–L1 treatment. Lastly, MOF/MSA-2(+)+αPD–L1 treatment increased γ-H2AX expression and reduced the cell proliferation marker Ki67 signal (Figure 6b).[26] Taken together, the synergistic actions of MOF-mediated RT, STING activation by MSA-2, and immune checkpoint blockade by αPD–L1 induce an inflammatory TME and trigger adaptive immune responses over time.

Radiosensitizers enhance the efficacy of RT by increasing the DNA damage of radiation to cancer cells.[27] This DNA damage effect reduces the required radiation dose for cure and mitigates toxicity in patients. Hafnium oxide nanoparticles and nanoscale MOFs[28] are currently under clinical evaluation as radiosensitizers. By leveraging high-Z elements, they absorb more X-rays to generate more ROS and cause more DNA damage.[29] Additionally, nanoscale MOFs also trigger ICD to release TAAs and DAMPs,[30] leading to an immunostimulatory TME.

Synthetic STING agonists activate the STING pathway by mimicking the action of endogenous 2′3′-cyclic GMP-AMP (cGAMP)[31] to induce the production of IFN-β and other inflammatory cytokines by immune cells, which enhances the immune system′s ability to recognize and eliminate cancer cells. However, the development of STING agonists such as MSA-2 has faced significant challenges. For

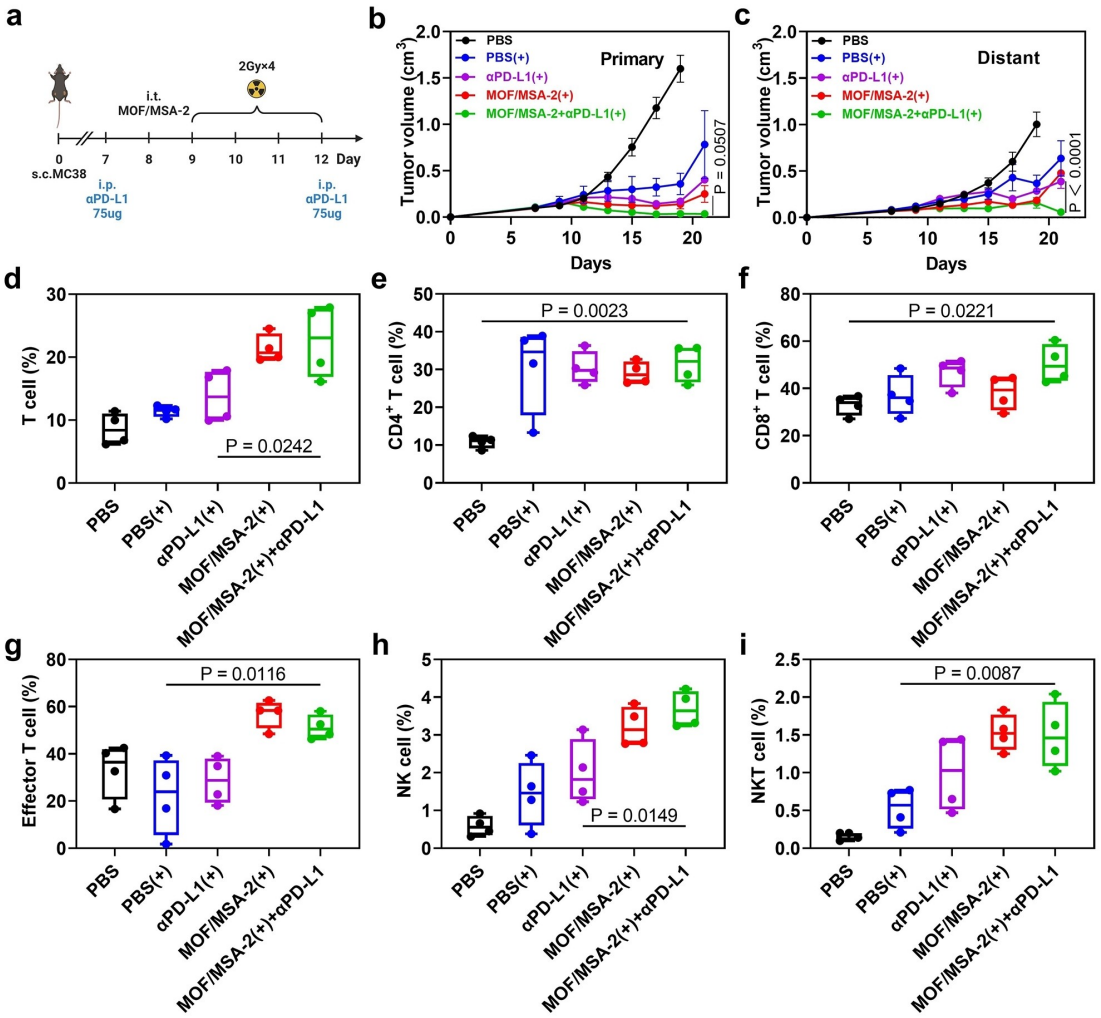

Figure 5. (a) Scheme showing tumor inoculation and treatment schedules. Treatments were intratumorally injected and 2 Gy/fraction was given to the primary tumors on 4 consecutive days starting on day 8. Intraperitoneal (i.p.) injection of αPD–L1 (75 μg) was given on day 7 and 12. (b,c) Growth curves of treated primary tumors (b) and untreated distant tumors (c) on a bilateral subcutaneous MC38 tumor model in C57BL/6 mice. (d–i) Immune cell infiltration into primary tumors on day 17 (5 days after the last dose of X-ray) quantified by flow cytometry. T cell subpopulations are defined as: (d) Total T cells as $CD45^+CD3e^+$; (e) $CD4^+$ cells as $CD45^+CD3e^+CD4^+$; (f) $CD8^+$ T cells as $CD45^+CD3e^+CD8^+$; (g) Effector T cells as $CD45^+CD3e^+CD44^+CD62\,L^-$; (h) NK cells as $CD45^+CD3e^-NK1.1^+$; (i) NKT cells as $CD45^+CD3e^+NK1.1^+$ (ANOVA with Tukey test, $n = 4$). The scheme was created with BioRender.com.

example, a major hurdle is the effective and sustained delivery of these STING agonists to the TME. We have leveraged the coordination of MSA-2 to Hf_6 SBUs in MOF/MSA-2 to selectively release MSA-2 in the TME. We observed a markedly increased and sustained release of MSA-2 from MOF/MSA-2 in a high phosphate concentration that mimics intracellular environments. As a result, MOF/MSA-2 elicits potent and sustained STING activation to lead to a highly inflammatory TME (Figure 6c).

MOF-mediated RT and STING activation by MSA-2 showed strong synergy in regressing colorectal tumors in mouse models at a low X-ray dose of 2 Gy/fraction for 3 or 4 daily fractions and a low MSA dose of 0.5 mg per mouse. Immune profiling studies showed that MOF/MSA-2(+) enhances inflammatory responses in the TME and TDLNs to recruit and activate innate immune cells in the short term and increases intratumoral infiltration of $CD8^+$, $CD4^+$, and effector T cells, NK cells, and NKT cells in the long term to trigger potent anti-tumor immunity. Further combination of MOF/MSA-2(+) with αPD–L1 improves distant tumor control to elicit an abscopal effect on a bilateral tumor model, thus extending the local therapeutic effect of MOF/MSA-2(+) to systemic antitumor immune responses.

Conclusions

In this work, we developed a bifunctional MSA-2 conjugated nanoscale MOF that serves as both a radiosensitizer and an immunostimulant. The MOF increases the sensitivity of cancer cells to X-ray irradiation by enhancing ROS generation and DNA damage as well as inducing ICD of cancer

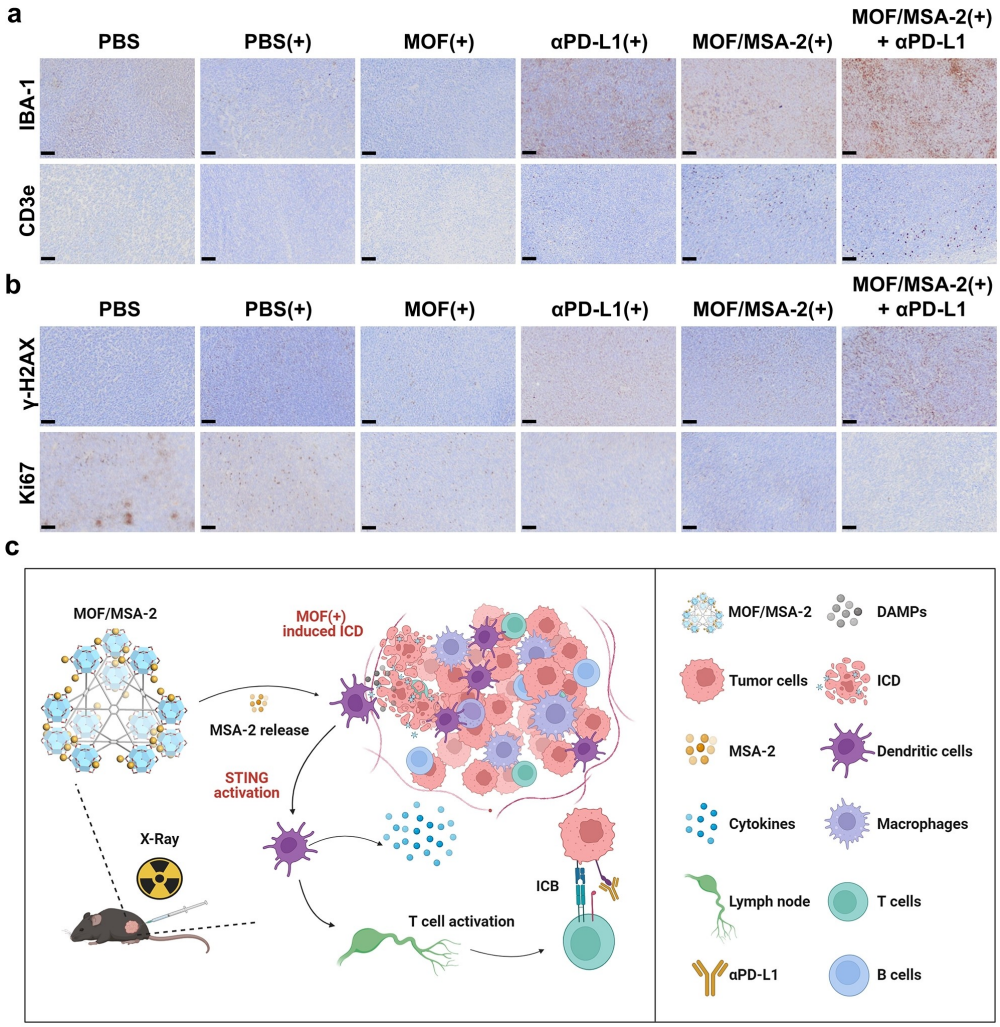

Figure 6. (a) Immunohistochemistry of pan-macrophage cells with IBA-1 staining (top) and T cells with CD3e staining (bottom) in primary tumors. (b) Immunohistochemistry with γ-H2AX staining (top) and Ki67 staining (bottom) in primary tumors. All scale bars are 100 μm. (c) Mechanistic summary of synergistic radiosensitization and immune activation by MOF/MSA-2(+). MOF/MSA-2 functions as a powerful radiosensitizer and delivers MSA-2 for STING activation to promote cancer immunotherapy. RT activates the MOF to mediate ICD of cancer cells to release TAAs and DAMPs while the released MSA-2 elicits potent and sustained STING activation in macrophages and DCs. The activated APCs secrete type I IFN and inflammatory cytokines for recruitment and stimulation of infiltrating leukocytes, resulting in enhanced tumor antigen presentation and the activation of antitumor immunity. The combination of MOF/MSA-2(+) with αPD–L1 improves distant tumor control to elicit an abscopal effect and extends the local therapeutic effect to systemic antitumor immunity. The scheme was created with BioRender.com.

cells to trigger the release of TAAs and DAMPs. MOF/MSA-2 significantly enhances the uptake and retention of MSA-2 in the TME to elicit robust and sustained STING activation, leading to a highly inflammatory TME. The synergistic actions of MOF-mediated RT and STING activation by MSA-2 regress local tumors and activate the tumor immune environment on two murine colon cancer models. The combination of MOF/MSA-2 plus low doses of X-rays with αPD–L1 improves distant tumor control to elicit an abscopal effect on a bilateral tumor model of CRC via systemic antitumor immune responses. Our work establishes MOFs as a promising nano-platform for simultaneous STING activation and radiosensitization, and given the synthetic tunability of MOFs, we envision the development of novel multifunctional MOF conjugates for effective cancer immunotherapy.

Supporting Information

The authors have cited additional references within the Supporting Information.

Acknowledgements

We acknowledge funding from the National Cancer Institute (1R01CA253655).

Conflict of Interest

W.L. is the founder of Coordination Pharmaceuticals, which licensed the MOF technology from the University of Chicago. R.R.W. is an advisor to Coordination Pharmaceuticals.

Data Availability Statement

The data that support the findings of this study are available from the corresponding author upon reasonable request.

Keywords: metal–organic frameworks · STING agonist · radiotherapy · radiosensitization · cancer immunotherapy

[1] W. Zhen, R. R. Weichselbaum, W. Lin, *Adv. Mater.* **2023**, *35*, e2206370.

[2] a) X. Jiang, T. Luo, K. Yang, M. J. Lee, J. Liu, L. Tillman, W. Zhen, R. R. Weichselbaum, W. Lin, *Sci. Adv.* **2024**, *10*, eado0082; b) M. Krause, A. Dubrovska, A. Linge, M. Baumann, *Adv. Drug Delivery Rev.* **2017**, *109*, 63; c) M. A. Olivares-Urbano, C. Griñán-Lisón, J. A. Marchal, M. I. Núñez, *Cells-Basel* **2020**, *9*; d) M. Diehn, M. F. Clarke, *J. Natl. Cancer Inst.* **2006**, *98*, 1755.

[3] S. C. Formenti, S. Demaria, *Lancet Oncol.* **2009**, *10*, 718.

[4] a) J. Zhang, M. Yang, X. Fan, M. Zhu, Y. Yin, H. Li, J. Chen, S. Qin, H. Zhang, K. Zhang, F. Yu, *J. Nanobiotechnol.* **2022**, *20*, 103; b) Z. Konsoula, A. Velena, R. Lee, A. Dritschilo, M. R. Jung, *Adv. Exp. Med. Biol.* **2012**, *720*, 171; c) S. K. R. Noonepalle, S. Grindrod, N. Aghdam, X. T. Li, M. Gracia-Hernandez, C. Zevallos-Delgado, M. R. Jung, A. Villagra, A. Dritschilo, *Mol. Cancer Ther.* **2023**, *22*, 1376; d) B. L. Cline, W. Jiang, C. B. Lee, Z. W. Cao, X. Y. Yang, S. Y. Zhan, H. Chong, T. Zhang, Z. G. Han, X. D. Wu, L. Yao, H. Wang, W. Z. Zhang, Z. B. Li, J. Xie, *ACS Nano* **2021**, *15*, 17401.

[5] a) H. E. Barker, J. T. Paget, A. A. Khan, K. J. Harrington, *Nat. Rev. Cancer* **2015**, *15*, 409; b) H. Liang, L. Deng, Y. Hou, X. Meng, X. Huang, E. Rao, W. Zheng, H. Mauceri, M. Mack, M. Xu, Y. X. Fu, R. R. Weichselbaum, *Nat. Commun.* **2017**, *8*, 1736.

[6] B. T. Oronsky, S. J. Knox, J. Scicinski, *Transl. Oncol.* **2011**, *4*, 189.

[7] a) Z. Kuncic, S. Lacombe, *Phys. Med. Biol.* **2018**, *63*, 02TR01; b) Z. Xu, K. Ni, J. Mao, T. Luo, W. Lin, *Adv. Mater.* **2021**, *33*, e2104249.

[8] M. Koshy, M. Spiotto, L. E. Feldman, J. J. Luke, G. F. Fleming, D. Olson, J. W. Moroney, R. Nanda, A. Rosenberg, A. T. Pearson, A. Juloori, F. Weinberg, C. Ray, R. C. Gaba, P. J. Chang, L. A. Janisch, Z. Q. Xu, W. Lin, R. R. Weichselbaum, S. J. Chmura, *J. Clin. Oncol.* **2023**, *41*.

[9] a) M. Yi, M. Niu, Y. Wu, H. Ge, D. Jiao, S. Zhu, J. Zhang, Y. Yan, P. Zhou, Q. Chu, K. Wu, *J. Hematol. Oncol.* **2022**, *15*, 142; b) B. S. Pan, S. A. Perera, J. A. Piesvaux, J. P. Presland, G. K. Schroeder, J. N. Cumming, B. W. Trotter, M. D. Altman, A. V. Buevich, B. Cash, S. Cemerski, W. Chang, Y. Chen, P. J. Dandliker, G. Feng, A. Haidle, T. Henderson, J. Jewell, I. Kariv, I. Knemeyer, J. Kopinja, B. M. Lacey, J. Laskey, C. A. Lesburg, R. Liang, B. J. Long, M. Lu, Y. Ma, E. C. Minnihan, G. O'Donnell, R. Otte, L. Price, L. Rakhilina, B. Sauvagnat, S. Sharma, S. Tyagarajan, H. Woo, D. F. Wyss, S. Xu, D. J. Bennett, G. H. Addona, *Science* **2020**, *369*; c) S. Crunkhorn, *Nat. Rev. Drug Discovery* **2020**, *19*, 669.

[10] X. A. Chen, F. C. Meng, Y. T. Xu, T. Y. Li, X. L. Chen, H. X. Wang, *Nat. Commun.* **2023**, *14*.

[11] a) L. Zeng, S. Ding, Y. Cao, C. Li, B. Zhao, Z. Ma, J. Zhou, Y. Hu, X. Zhang, Y. Yang, G. Duan, X. W. Bian, G. Tian, *ACS Nano* **2023**, *17*, 13195; b) T. Luo, X. Jiang, Y. Fan, E. Yuan, J. Li, L. Tillman, W. Lin, *Natl. Sci. Rev.* **2024**, *11*, nwae167; c) Z. Xu, W. Zhen, C. McCleary, T. Luo, X. Jiang, C. Peng, R. R. Weichselbaum, W. Lin, *J. Am. Chem. Soc.* **2023**, *145*, 18698; d) K. Lu, C. He, N. Guo, C. Chan, K. Ni, G. Lan, H. Tang, C. Pelizzari, Y. X. Fu, M. T. Spiotto, R. R. Weichselbaum, W. Lin, *Nat. Biomed. Eng.* **2018**, *2*, 600; e) K. Y. Ni, G. X. Lan, C. Chan, B. Quigley, K. D. Lu, T. Aung, N. N. Guo, P. La Riviere, R. R. Weichselbaum, W. B. Lin, *Nat. Commun.* **2018**, *9*; f) K. Ni, T. Luo, A. Culbert, M. Kaufmann, X. Jiang, W. Lin, *J. Am. Chem. Soc.* **2020**, *142*, 12579.

[12] M. Zhu, M. Yang, J. Zhang, Y. Yin, X. Fan, Y. Zhang, S. Qin, H. Zhang, F. Yu, *Front. Immunol.* **2021**, *12*, 705361.

[13] a) D. Alezi, I. Spanopoulos, C. Tsangarakis, A. Shkurenko, K. Adil, Y. Belmabkhout, O. K. M, M. Eddaoudi, P. N. Trikalitis, *J. Am. Chem. Soc.* **2016**, *138*, 12767; b) J. S. Qin, S. Yuan, L. Zhang, B. Li, D. Y. Du, N. Huang, W. Guan, H. F. Drake, J. Pang, Y. Q. Lan, A. Alsalme, H. C. Zhou, *J. Am. Chem. Soc.* **2019**, *141*, 2054.

[14] Y. Song, Y. Pi, X. Feng, K. Ni, Z. Xu, J. S. Chen, Z. Li, W. Lin, *J. Am. Chem. Soc.* **2020**, *142*, 6866.

[15] C. Koschnick, R. Staglich, T. Scholz, M. W. Terban, A. von Mankowski, G. Savasci, F. Binder, A. Schokel, M. Etter, J. Nuss, R. Siegel, L. S. Germann, C. Ochsenfeld, R. E. Dinnebier, J. Senker, B. V. Lotsch, *Nat. Commun.* **2021**, *12*, 3099.

[16] a) C. Wang, R. Zhang, J. He, L. Yu, X. Li, J. Zhang, S. Li, C. Zhang, J. C. Kagan, J. M. Karp, R. Kuai, *Nat. Commun.* **2023**, *14*, 3877; b) X. Li, J. Gao, C. Wu, C. Wang, R. Zhang, J. He, Z. J. Xia, N. Joshi, J. M. Karp, R. Kuai, *Sci. Adv.* **2024**, *10*, eadl0479.

[17] T. Luo, G. T. Nash, X. Jiang, X. Feng, J. Mao, J. Liu, A. Juloori, A. T. Pearson, W. Lin, *Adv. Mater.* **2022**, *34*, e2110588.

[18] X. Zhao, Y. Li, L. Du, Z. Deng, M. Jiang, S. Zeng, *Adv. Healthcare Mater.* **2021**, *10*, e2101174.

[19] J. Y. Lim, S. A. Gerber, S. P. Murphy, E. M. Lord, *Cancer Immunol. Immunother.* **2014**, *63*, 259.

[20] C. T. Wu, M. F. Chen, W. C. Chen, C. C. Hsieh, *Radiat. Oncol.* **2013**, *8*, 159.

[21] R. S. A. Goedegebuure, C. Vonk, L. P. Kooij, S. Derks, V. Thijssen, *Int. J. Radiat. Oncol. Biol. Phys.* **2020**, *108*, 56.

[22] G. N. Barber, *Nat. Rev. Immunol.* **2015**, *15*, 760.

[23] D. Shae, K. W. Becker, P. Christov, D. S. Yun, A. K. R. Lytton-Jean, S. Sevimli, M. Ascano, M. Kelley, D. B. Johnson, J. M. Balko, J. T. Wilson, *Nat. Nanotechnol.* **2019**, *14*, 269.

[24] L. Galluzzi, M. J. Aryankalayil, C. N. Coleman, S. C. Formenti, *Nat. Rev. Clin. Oncol.* **2023**, *20*, 543.

[25] a) A. M. Stessin, M. G. Clausi, Z. Zhao, H. Lin, W. Hou, Z. Jiang, T. Q. Duong, S. E. Tsirka, S. Ryu, *J. Neuro-Oncol.* **2020**, *147*, 547; b) T. Kordbacheh, J. Honeychurch, F. Blackhall, C. Faivre-Finn, T. Illidge, *Ann. Oncol.* **2018**, *29*, 301.

[26] a) A. Pollack, D. Cowen, P. Troncoso, G. K. Zagars, A. C. von Eschenbach, M. L. Meistrich, T. McDonnell, *Cancer* **2003**, *97*, 1630; b) T. O. Nielsen, S. C. Y. Leung, N. Riaz, A. M. Mulligan, Z. Kos, A. Bane, T. J. Whelan, *Histopathology* **2023**, *83*, 903; c) J. Kao, M. T. Milano, A. Javaheri, M. C. Garofalo, S. J. Chmura, R. R. Weichselbaum, S. J. Kron, *Curr. Cancer Drug Targets* **2006**, *6*, 197; d) R. Wan, Y. Mo, R. Tong, M. Gao, Q. Zhang, *Methods Mol. Biol.* **2019**, *1894*, 145.

[27] P. Wardman, *Clin. Oncol.-Uk* **2007**, *19*, 397.

[28] Y. Zhao, C. Liang, Z. J. Mei, H. X. Yang, B. Wang, C. H. Xie, Y. Xu, J. Tian, *ACS Materials Lett.* **2023**, *5*, 3237.

[29] R. X. Huang, P. K. Zhou, *Signal Transduct. Tar.* **2020**, *5*.

[30] a) K. Zhang, Z. Yang, X. Mao, X. L. Chen, H. H. Li, Y. Y. Wang, *ACS Appl. Mater. Interfaces* **2020**, *12*, 55316; b) H. L. Hu, Z. C. Dai, F. F. Zhang, C. L. Xin, Q. An, X. Y. Meng, Z. F. Hu, W. J. Wang, L. Tian, X. W. Zheng, *Chem. Eng. J.* **2024**, *479*; c) Z. Z. Feng, G. Chen, M. Zhong, L. Lin, Z. Y. Mai, Y. Tang, G. M. Chen, W. Ma, G. Li, Y. Y. Yang, Z. Q. Yu, M. Yu, *Biomaterials* **2023**, *302*; d) O. Kutuk, N. Aytan, B. Karakas, A. G. Kurt, U. Acikbas, S. G. Temel, H. Basaga, *PLoS One* **2017**, *12*; e) J. Yang, X. Y. Zhao, M. Tang, L. Li, Y. Lei, P. Cheng, W. H. Guo, Y. Zheng, W. Wang, N. Luo, Y. Peng, A. P. Tong, Y. Q. Wei, C. L. Nie, Z. Yuan, *Oncotarget* **2017**, *8*, 23492.

[31] S. T. Koshy, A. S. Cheung, L. Gu, A. R. Graveline, D. J. Mooney, *Adv. Biosyst.* **2017**, *1*.

Manuscript received: September 4, 2024
Accepted manuscript online: October 7, 2024
Version of record online: ■■, ■■

Research Article

Cancer Therapy

C. Wang, J. Li, X. Jiang, X. Ma, W. Zhen, L. Tillman, R. R. Weichselbaum,* W. Lin* _____ **e202417027**

Bifunctional Metal–Organic Framework Synergistically Enhances Radiotherapy and Activates STING for Potent Cancer Radio-Immunotherapy

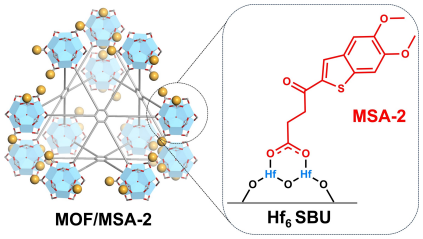

A bifunctional nanoscale metal–organic framework (MOF), MOF/MSA-2, leverages high-Z Hf_6 secondary building units for radioenhancement and releases MSA-2 for sustained STING activation to mediate the regression of colon tumors in mice. Further combination with immune checkpoint blockade effectively suppresses both primary and distant tumors through systemic immune activation.